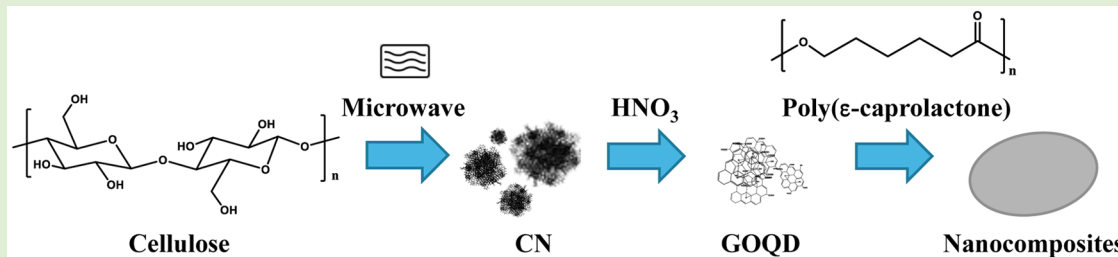


# Supramolecular Assembly of Biobased Graphene Oxide Quantum Dots Controls the Morphology of and Induces Mineralization on Poly( $\epsilon$ -caprolactone) Films

Salman Hassanzadeh, Karin H. Adolfsson, Duo Wu, and Minna Hakkarainen\*

Department of Fiber and Polymer Technology, KTH Royal Institute of Technology, SE-100 44 Stockholm, Sweden



**ABSTRACT:** Biobased 2D graphene oxide quantum dots (GOQDs) were synthesized from waste paper via carbon nanosphere intermediates and evaluated as property-enhancing additives for poly( $\epsilon$ -caprolactone) (PCL). The morphology of PCL films was controlled by supramolecular assembly of the small, 2D GOQDs in the polymer matrix. Phase behavior studies of PCL-GOQD in the solid state indicated concentration-dependent self-association of GOQD sheets, which was confirmed by SEM observations. Depending on the GOQD concentration, the formation of, e.g., spheres and stacked sheets was observed. GOQDs also induced mineralization on the surface of the films. A calcium phosphate (CaP) mineralization test revealed that the density of growing CaP crystals was controlled by the type of GOQD aggregates formed. Thus, utilization of the aggregation behavior of small GOQD sheets in polymeric matrices paves the way for tuning the morphology and properties of nanocomposites.

## INTRODUCTION

Combining polymeric materials with graphene-based structures has resulted in a library of structurally engineered composites.<sup>1–3</sup> Graphene oxide (GO), as a 2D sheet with  $\text{sp}^3$  oxygenous functional edge groups surrounding the  $\text{sp}^2$  core, has a beneficial structure for premixing with other materials.<sup>4</sup> It has been shown that GO has favorable interactions with several polymer matrices and accordingly can influence the properties and intrachain ordering of semicrystalline chains.<sup>5,6</sup> As an example, blending GO with poly(vinyl alcohol) (PVA),<sup>7</sup> poly(propylene carbonate),<sup>8</sup> or cross-linked poly(propylene fumarate)<sup>9</sup> led to largely enhanced mechanical properties.

Polylactide (PLA)/GO composites were investigated by several groups.<sup>10</sup> A low concentration of GO in a poly(L-lactide) (PLLA) matrix led to an accelerated crystallization rate due to the nucleating function of GO.<sup>11</sup> At concentrations higher than 1 wt %, a GO network was formed that restricted the mobility and diffusion of PLA chains. Another study evaluated the role of size and structural integrity in the nucleation ability of reduced graphene oxide (rGO).<sup>12</sup> A highly interesting effect was observed in PLA stereocomplex materials, where GO selectively induced stereocomplex crystallization.<sup>13,14</sup> This phenomenon resulted in greatly improved gas barrier properties and thermal stability, i.e., GO decorated with stereocomplex crystals functioned as thermostable and impermeable walls in the material.

A series of papers evaluated the preparation of PCL/GO and PCL/rGO composites with covalently attached GO or rGO to

improve the dispersion of GO and rGO in the PCL matrix.<sup>15–17</sup> Covalent anchoring of PCL chains to graphene sheets resulted in a doubling of Young's modulus and tensile strength as well as a large increase in electrical conductivity compared to that of pristine PCL.<sup>16</sup> A low concentration of rGO (<1 wt %) did not change the enzymatic degradation rate of PCL/rGO composites.<sup>18</sup> However, inconsistent rGO loss was observed for composites containing free rGO, whereas composites with covalently attached rGO retained their PCL/rGO composition during the degradation experiment. The biocompatible and nontoxic nature of both PCL and GO also makes PCL/GO composites highly interesting for various biomedical applications.<sup>19</sup>

Recently, we developed a one-pot synthesis of 3D carbon nanospheres (CNs) and green chemicals through the microwave-assisted hydrothermal degradation of cellulose,<sup>20</sup> waste paper,<sup>21</sup> and starch.<sup>22</sup> The synthesized amorphous CNs with an unordered domain of graphitic flakes were utilized as precursors in the preparation of small 2D graphene oxide quantum dots (GOQDs) via an oxidation reaction.<sup>23</sup> The lateral diameter of the synthesized GOQD was only 1–3 nm, while at the same time, the oxygen content was unusually high. This gives excellent prerequisites for obtaining good dispersion in polymer matrices through the formation of noncovalent interactions

Received: October 6, 2015

Revised: December 7, 2015

Published: December 9, 2015

between polymers, like polyesters and GOQDs. We also revealed a fascinating concentration- and pH-dependent self-assembly behavior of 2D GOQD single sheets in aqueous solutions.<sup>24</sup> If a similar concentration-dependent self-assembly takes place when GOQDs are embedded in a polymer matrix, then this could be utilized to tune the morphology and properties of the resulting composite films. In addition, GOQDs, due to their inherent properties, could introduce highly valuable properties, such as mineralization and fluorescence, to the composites.

## EXPERIMENTAL SECTION

**Chemicals.** PCL ( $M_n = 70\,000$  g/mol), sulfuric acid ( $H_2SO_4$ , 95–98%), nitric acid ( $HNO_3$ , 70%), and sodium hydroxide ( $NaOH$ , 97%) were purchased from Sigma-Aldrich Chemie GmbH (Steinheim, Germany). Acetone (ACS reagent, ≥99.5%) was purchased from Fisher scientific. The cellulose-rich waste product was brown paper tissue (BT) (KATRIN Basic; 25 × 20.6 cm<sup>2</sup>). All other reagents and solvents were of AR grade and used as received without further purification. Distilled water was used throughout.

**Synthesis of GOQDs.** The synthesis and characteristics of GOQDs, produced from CNs synthesized by microwave-assisted hydrothermal recycling of cellulose in waste paper,<sup>20,21</sup> were in accordance with those in our previous paper.<sup>23</sup> The average diameter of a GOQD was 2–3 nm according to dynamic light scattering.<sup>23</sup> A 15 mL solution of waste paper-based CNs in  $HNO_3$  (1:100, w/w) was put in a 100 mL one-necked round-bottomed flask, sonicated at 45 °C for 30 min, and heated for 30 min at 90 °C. Fifty milliliters of deionized  $H_2O$  (15 °C) was added to the solution to stop the reaction. The acidic  $H_2O$  was removed by rotary evaporation, resulting in an orange/red solid powder of GOQDs. The synthesized GOQDs were kept in a vacuum oven for 1 week to remove any other trapped  $H_2O$  and acid residues.

**PCL-GOQD Film Preparation.** Solution casting was used for the preparation of films. Thirty milligrams of PCL and 0, 0.25, 1.0, 2.5, or 7.5 wt % of GOQD were dissolved in 1 mL of dry acetone. The solutions were then sonicated for 5 min in a sonication bath (Bransonic Ultrasonic cleaners, model 2210, 40 kHz, 130 W at  $T = 50$  °C). The solutions were casted on dust-free Petri dishes and dried at room temperature for 3 days, after which the films were kept in a vacuum oven for 24 h at room temperature to evaporate any residual acetone. All films were kept in desiccators for further characterization. The films were named according to the percentage of GOQD as follows: PCL0 (pure PCL), PCL0.25 (0.25 wt % of GOQDs), PCL1.0 (1 wt % of GOQDs), PCL2.5 (2.5 wt % of GOQDs), and PCL7.5 (7.5 wt % of GOQDs). The mean thickness measured for all films was ~50 μm.

**Thermal Analysis.** Differential scanning calorimetry (DSC) analyses were performed on a Metter-Toledo DSC 820. Around 5 mg of sample was placed into standard 100 μL aluminum cups with a pinhole, and the temperature was increased at 10 °C/min in a  $N_2$  atmosphere (flow rate of 50 mL/min). The same preparation and parameters were used for all of the films, and the temperature program was set to go from –70 to 100 °C, then to –70 °C, and up to 100 °C again. The weight percent of crystallinity ( $X_c$ ) was obtained from eq 1.

$$X_c (\%) = \frac{\Delta H_f(T_m)}{\Delta H^\circ_f(T_m)} \cdot 100 \quad (1)$$

$\Delta H_f$  is the enthalpy of fusion at  $T_m$ , and  $\Delta H^\circ_f$  is the enthalpy of fusion for crystalline PCL (139.3 J/g)<sup>25</sup> at  $T_m$ .

**FTIR Imaging.** PCL-GOQD films were studied by FTIR imaging. FTIR imaging analyses were performed in attenuated total reflectance mode on a Spectrum Spotlight 400 FTIR microscope connected to a Spectrum 100 FTIR spectrometer (PerkinElmer Inc.). The images were taken at a resolution of 8 cm<sup>–1</sup> between 4000 and 600 cm<sup>–1</sup> with 16 scans per pixel.

**Scanning Electron Microscopy (SEM).** Ultra-high-resolution FE-SEM (Hitachi S-4800) was used to study the surface morphology of

the prepared films. PCL nanocomposites were sputtered with a 3 nm thick platinum/palladium layer before the SEM observations were performed. Energy dispersive X-ray spectroscopy (EDS) spectra were acquired on the same Hitachi S-4800 SEM, equipped with an Oxford Instruments X-MaxN 80 EDS at a voltage of 15kV.

**Wide-Angle X-ray Scattering (WAXS).** X-ray diffraction (XRD) was recorded for the PCL-GOQD films in the wide 2θ angular range between 5 and 55°. The X-ray source was Cu Kα radiation ( $\lambda = 0.1541$  nm), and the diffraction was measured by a PANalytical X'pert PRO diffractometer at 25 °C with a silicon monocrystal sample holder with a step size of 0.017° for all analyses. The estimation of the PCL crystallite size ( $D$ ) was obtained at the [110] crystallographic plane using the Scherrer equation.<sup>26</sup>

$$D (\text{nm}) = \frac{K\lambda}{\Delta 2\theta \cos \theta} \quad (2)$$

where  $\Delta 2\theta$  is the full width at half-maximum,  $\theta$  is the maximum point in radians,  $K$  is the Scherrer constant (0.9), and  $\lambda$  is the X-ray wavelength.

**Polarized Optical Microscopy (POM).** A Leitz Ortholux POL BK II optical microscope equipped with crossed polarizers was used to visualize crystals in the films. Specimens were prepared in acetone and solution-cast onto glass slides, which were left to dry at room temperature. The microscopic images were recorded under isothermal conditions by a Leica DC 300 CCD camera.

**Incubation of PCL-GOQD in Simulated Body Fluids.** For the mineralization test, PCL0, PCL0.25, and PCL7.5 were cut into 0.5 × 0.5 cm<sup>2</sup> square films and immersed in 40 mL of simulated body fluid (SBF) in a polystyrene beaker according to a previously reported procedure.<sup>27,28</sup> Briefly, the films were incubated in an oven at 37 ± 0.5 °C and the SBF solution was refreshed every day. A conventional SBF solution was prepared as follows: NaCl (7.996 g/L), NaHCO<sub>3</sub> (0.350 g/L), KCl (0.224 g/L), K<sub>2</sub>HPO<sub>4</sub>·3H<sub>2</sub>O (0.228 g/L), MgCl<sub>2</sub>·6H<sub>2</sub>O (0.305 g/L), HCl (1 mol/L, 40 mL), CaCl<sub>2</sub> (0.278 g/L), Na<sub>2</sub>SO<sub>4</sub> (0.071 g/L), and tris(hydroxymethyl) aminomethane (Tris, 6.057 g/L). The concentrations of different ions were as follows: Na<sup>+</sup>, 142; Ca<sup>2+</sup>, 5.0; Mg<sup>2+</sup>, 1.5; Ca<sup>2+</sup>, 2.5; Cl<sup>–</sup>, 147.8; HCO<sup>3–</sup>, 4.2; HPO<sub>4</sub><sup>2–</sup>, 1.0; and SO<sub>4</sub><sup>2–</sup>, 0.5 mmol/L at a pH of 7.4, equating to conditions in human blood plasma. After incubation for 2 weeks, the films were taken out and thoroughly rinsed with distilled water three times to remove any free ions. The films were dried at room temperature before FTIR imaging and SEM characterization.

## RESULTS AND DISCUSSION

Recently, we developed a novel process for the production of biobased GOQDs from low-quality paper waste.<sup>23</sup> Here, we evaluate the waste-paper-derived GOQDs as a potential functional filler in PCL with the aim of influencing the crystallization process and inducing mineralization on the films.

**Initial Characterization of PCL Nanocomposites.** The characteristic peaks of the GOQDs were observed in the FTIR spectra of the final films with different absorption intensities depending on the GOQD content (Figure 1). Stretching of acidic and phenolic OH, a broad peak from 2500 to 3500 cm<sup>–1</sup>, and stretching of C=C, a shoulder for carbonyl peak at ~1650 cm<sup>–1</sup>, were assigned as originating from the GOQDs. The intensity of these peaks consequently increased as the concentration of GOQDs increased.

**Surface Microstructures.** The microstructures of the surfaces of the prepared films were monitored by SEM. The images illustrate clear differences in the morphologies of the films containing different concentrations of GOQDs. While disordered PCL lamellae were distinguishable in PCL0, PCL1.0, and PCL7.5, it seems that ordered lamellae in PCL0.25 and PCL2.5 formed spherulites with approximate diameters of 50 μm (Figure 2). As the GOQD concentration increased, the tendency of single QDs to associate resulted in

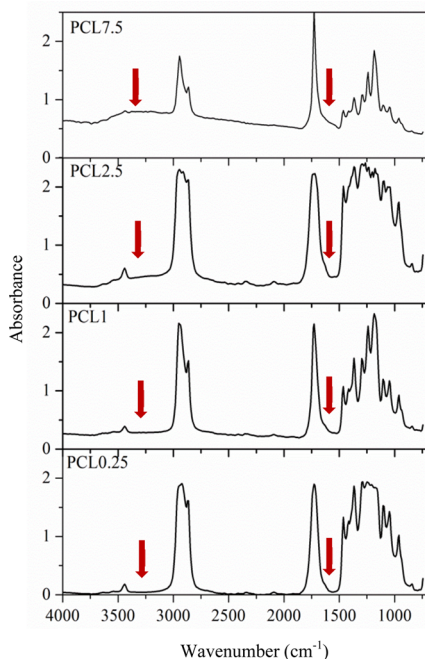


**Figure 1.** FTIR spectra of PCL-GOQD films with different GOQD concentrations.

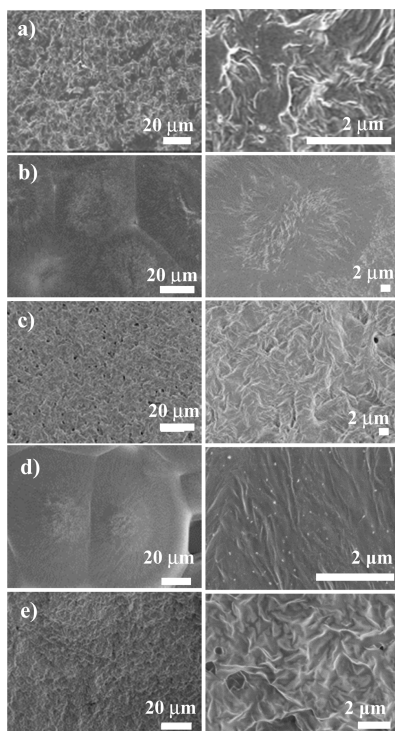


**Figure 2.** SEM images of PCL0 (a), PCL0.25 (b), PCL1.0 (c), PCL2.5 (d), and PCL7.5 (e).

the formation of spherical nanoparticles with sizes  $<100$  nm in PCL2.5. Interestingly, in PCL7.5, spherical nanoparticles were not observed; instead, GOQDs seemed to assemble into stacked nanosheets.

**Phase Behavior.** The phase behavior and crystallinity of PCL nanocomposites were evaluated by DSC (Table 1). PCL0.25 and PCL2.5 both had a significantly lower initial crystallinity as compared to that of PCL0. This together with

**Table 1. Thermal Properties of PCL Nanocomposites**

sample	$X_{cl}^a$ (%)	$T_{m1}^b$ (°C)	$T_c^c$ (°C)	$T_o^d$ (°C)	$X_{c2}^e$ (%)	$T_{m2}^f$ (°C)
PCL0	59.0	66.3	26.5	33.1	33.8	57.8
PCL0.25	51.8	62.6	26.6	33.8	42.3	57.6
PCL1.0	57.3	64.4	28.5	35.8	44.9	56.9
PCL2.5	51.5	64.5	28.4	37.7	47.4	56.7
PCL7.5	71.3	62.6	26.3	37.1	44.9	54.6

<sup>a</sup>Crystallinity from the first heating. <sup>b</sup>Melting temperature from the first heating. <sup>c</sup>Crystallization temperature. <sup>d</sup>Onset temperature for crystallization. <sup>e</sup>Crystallinity from the second heating. <sup>f</sup>Melting temperature from the second heating.

the spherulitic structures observed in Figure 2 indicated that there is a lower nucleation density for the materials with well-dispersed GOQD (PCL0.25) or GOQD forming spherical self-assemblies (PCL2.5). PCL0 and PCL1.0 had similar original crystallinities, whereas PCL7.5 had, by far, the highest original crystallinity. No spherulitic structures were observed in the SEM images, indicating a higher nucleation density and smaller crystal structures in these materials. However, the non-isothermal recrystallization during the cooling step emphasized that the presence of GOQDs accelerated the crystallization process for PCL, leading to a higher degree of crystallinity ( $X_{c2}$ ), higher or similar crystallization temperatures ( $T_c$ ), and higher crystallization onset temperatures ( $T_o$ ) for all of the films containing GOQDs. The enhanced crystallization rate implies that GOQDs act as efficient nucleating agents, possibly due to noncovalent interactions with PCL chains, i.e., hydrogen bonding between the hydroxyl groups of GOQDs and the carbonyl groups in PCL, resulting in the chains being organized faster and easier. This agrees with earlier studies in which positioning the functional groups on the surface of the 2D structure of GO enhanced the interactions with polymer matrices and induced crystallization of the polymer chains.<sup>13,29</sup> Furthermore, the nucleating effect of GO has also consequently been shown to lead to a higher crystallization temperature.<sup>15,30</sup>

The crystallinity of the PCL nanocomposites was further investigated by WAXS. As seen in Figure 3, three crystalline diffraction peaks at  $2\theta = 21.6$ , 22.1, and 23.9 were recognized as the [110], [111], and [200] crystallographic planes of PCL, respectively. The presence of the diffraction corresponding to

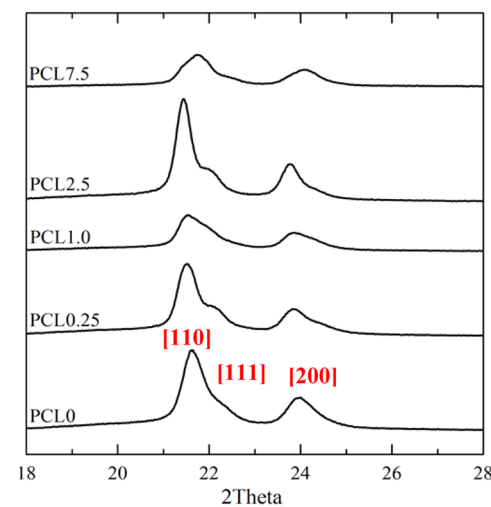


**Figure 3.** WAXS patterns of the prepared PCL-GOQD films.

the amorphous area at 21 indicates that the films are semicrystalline, as was also confirmed by DSC. There was a shift in the positions of the peaks to lower angles at [110] and [200] for PCL0.25 and PCL2.5 (which exhibit spherulitic structures) in comparison to those of pristine PCL, indicating that the crystalline state was less compact and that there were amorphous areas between the lamellae forming the spherulites, which further correlates with the lower overall crystallinity, as determined by DSC and WAXS (**Figure 4**). For PCL7.5, a shift

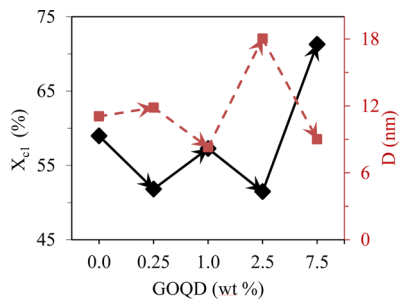


**Figure 4.** Degree of crystallinity from DSC (black squares) and crystal sizes from WAXS (red squares) measurements as a function of GOQD concentration.

to higher angles was observed, indicating in turn a more compact crystalline state, in accordance with the high overall crystallinity.<sup>31</sup> The peak broadening seen in PCL1.0 and PCL7.5 and less prominently in PCL0 indicated smaller crystallites in comparison to those for PCL0.25 and PCL2.5.

The morphologies in the PCL nanocomposites were further investigated by POM (**Figure 5**) by directly casting the

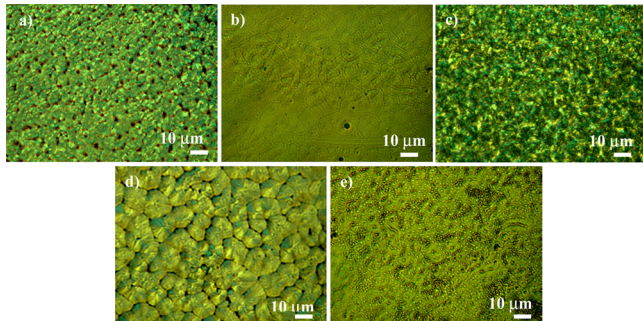


**Figure 5.** POM images of PCL0 (a), PCL0.25 (b), PCL1.0 (c), PCL2.5 (d), and PCL7.5 (e).

corresponding acetone solutions on glass slides. In accordance with the other results described, spherulites of ordered lamellae with boundaries were recognized in PCL0.25 and PCL2.5 due to the lower nucleation density. Smaller and imperfect crystal structures were formed in PCL1.0 and PCL7.5 materials, in which the nucleation density was higher, followed by rapid growth and contravention of neighboring crystals. Phase separation in PCL7.5 is visible as dark spots in **Figure 5e** and is explained by self-association of GOQDs, which was previously shown in solution.<sup>24</sup>

Furthermore, FTIR imaging was used to assess the homogeneity of the nanocomposites relative to the self-association tendency of GOQDs at different concentrations. Comparison of the esteric C=O of PCL at GOQD-rich and -poor areas of PCL7.5 films showed the formation of hydrogen bonds, with the hydroxyl groups of GOQDs acting as hydrogen

donors, resulting in a 3 cm<sup>-1</sup> red shift of the esteric C=O in GOQD-rich areas (**Figure 6**).

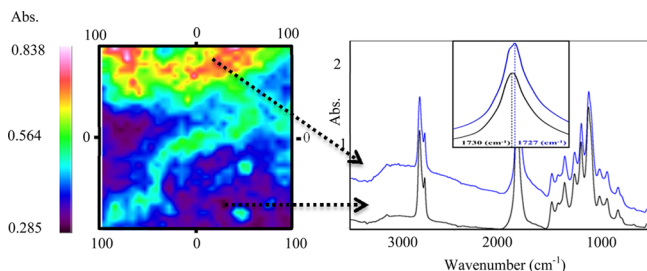


**Figure 6.** (Left) FTIR image of PCL7.5 film based on the absorption band at 3200 cm<sup>-1</sup> (hydroxyl group of GOQDs). (Right) FTIR spectra of different intensities in the image.

**GOQD's Ability To Promote Mineralization.** PCL is a well-known scaffold material for bone tissue engineering. In addition, the ability of GO to promote mineralization was recently reported.<sup>32</sup> A mineralization test was performed, therefore, on three samples (PCL0, PCL0.25, and PCL7.5) to evaluate the effect of the addition, concentration, and supramolecular structure of GOQDs on the bioactivity of the composites and to explore the potential of the prepared PCL nanocomposites as bone tissue scaffolds. The films were incubated in SBF at 37 °C and characterized after 2 weeks. **Figure 7a1–a3** shows FTIR images illustrating the absorption intensity at 1037 cm<sup>-1</sup> (PO<sub>4</sub><sup>2-</sup> absorption peak) on the surface of PCL after incubation in SBF. An obvious increase in the absorbance intensity was observed, which suggests that the concentration of PO<sub>4</sub><sup>2-</sup>, i.e., mineralization, increases with a higher content of GOQDs in the nanocomposites. Calcium phosphate (CaP) crystals could be induced on the PCL-GOQD surface because of the enhanced absorption of Ca<sup>2+</sup> on the hydrophilic carboxylic groups of GOQDs followed by phosphate group adsorption. The oxygen-containing functional groups in GO control the dispersion in composites and aqueous solutions. In addition, these functional groups act as anchor sites to induce mineralization in ion-containing fluids.<sup>33,34</sup> Therefore, the distribution, as well as the CaP crystal size, can provide further information about the dispersion and aggregation behavior of GOQDs in the PCL matrix. SEM images (**Figure 7**) revealed clearly that PCL makes no contribution to inducing CaP (**Figure 7b1**); both 0.25 and 7.5 wt % GOQDs, on the other hand, induced CaP crystal nucleation and growth on the film surface. The newly formed crystals showed a homogeneous distribution, which indicates that GOQDs were well-dispersed in the films (**Figure 7b2,b3**). While the density of CaP crystals on the surface of PCL0.25 films was higher, the sizes of CaP crystals on the surface of PCL7.5 films were larger. It seems that the supramolecular aggregation of GOQDs in PCL7.5 to form larger sheets will provide a lower number of nucleation centers with larger active surfaces (**Figure 7**, insets to b2 and b3). Furthermore, EDS confirmed that the crystals on the surface of PCL0.25 and PCL7.5 were mainly composed of Ca and P (**Figure 7c2,c3**). Trace amounts of Cl were also detected. The mineralization evaluation test demonstrated that PCL-GOQD is a promising bone scaffold material. In addition, it confirmed our other observations concerning the aggregation of small GOQDs to larger supramolecular structures depending on the GOQD concentration, which, in turn, influences the number of

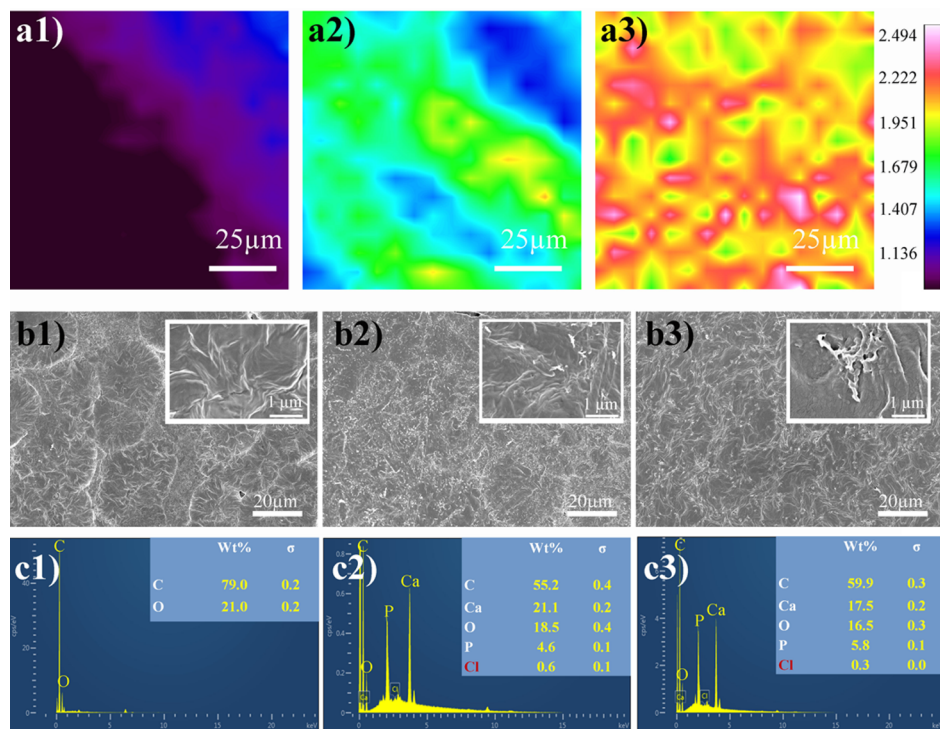


**Figure 7.** FTIR images ( $1037\text{ cm}^{-1}$ ,  $\text{PO}_4^{2-}$  stretching, single peak absorbance) of PCL0 (a1), PCL0.25 (a2), and PCL7.5 (a3); SEM images of PCL0 (b1), PCL0.25 (b2), and PCL7.5 (b3) films; and EDS spectra of PCL 0 (c1), PCL0.25 (c2), and PCL7.5 (c3) films after soaking in SBF for 14 days.

independent GOQD concentrated centers in different PCL-GOQD materials.

**Model for the Supramolecular Arrangement of GOQDs Facilitated by Their Concentration.** On the basis of the results, it can be concluded that a higher concentration of GOQDs enhanced the aggregation of GOQDs in the PCL matrix. The two competing intermolecular interactions between GOQD and GOQD or GOQD and PCL determined the dispersity and supramolecular structures of the GOQDs within the PCL matrix. At the same time, favorable interactions between PCL and GOQDs enabled the GOQDs to act as nucleating agents to induce PCL crystallization. This control over the supramolecular arrangement of the GOQD single sheets could be utilized to further tune the final properties of the prepared nanocomposites, e.g., crystallization and degree of crystallinity as well as mineralization properties. Images of small pieces of the prepared films under UV light (wavelength  $\sim 250\text{ nm}$ ) visually indicate the fluorescent property of the PCL nanocomposites and the dependence of this on the dispersion and self-assembly of GOQDs (Figure 8).

## CONCLUSIONS

2D GOQDs derived from waste paper were demonstrated to act as multifunctional property-enhancing additives for PCL, controlling the morphology and mineralization properties of

PCL films. Phase behavior studies of the PCL nanocomposites in the solid state indicated a concentration-dependent self-assembly of the GOQD sheets, which was directly reflected in the morphology of the PCL films. GOQDs also induced mineralization on the surface of PCL films. The self-assembly of GOQDs influenced the number of independent GOQD centers and tuned the number of nucleation points and subsequently the size and density of the formed CaP crystals. The structure–property relationships presented here provide a valuable toolbox for designing GOQD-based nanocomposites for wide range of potential applications.

## AUTHOR INFORMATION

### Corresponding Author

\*E-mail: minna@kth.se.

### Notes

The authors declare no competing financial interest.

## ACKNOWLEDGMENTS

The Swedish Research Council (VR) is acknowledged for financial support (contract grant number 2014-4091). D.W. is grateful to China Scholarship Council (CSC) for financial support.

## REFERENCES

- (1) Stankovich, S.; Dikin, D. A.; Domke, G. H. B.; Kohlhaas, K. M.; Zimney, E. J.; Stach, E. A.; Piner, R. D.; Nguyen, S. T.; Ruoff, R. S. Graphene-based composite materials. *Nature* **2006**, *442* (7100), 282–286.
- (2) Malho, J.-M.; Laaksonen, P.; Walther, A.; Ikkala, O.; Linder, M. B. Facile Method for Stiff, Tough, and Strong Nanocomposites by Direct Exfoliation of Multilayered Graphene into Native Nanocellulose Matrix. *Biomacromolecules* **2012**, *13* (4), 1093–1099.
- (3) Fan, H.; Wang, L.; Zhao, K.; Li, N.; Shi, Z.; Ge, Z.; Jin, Z. Fabrication, Mechanical Properties, and Biocompatibility of Graphene-

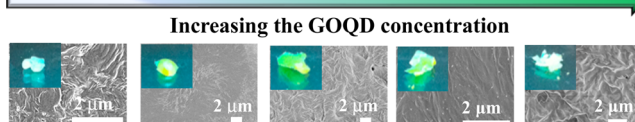


**Figure 8.** Images of the films under UV light ( $250\text{ nm}$ ) along with their corresponding SEM images.

- Reinforced Chitosan Composites. *Biomacromolecules* **2010**, *11* (9), 2345–2351.
- (4) Cote, L. J.; Cruz-Silva, R.; Huang, J. Flash Reduction and Patterning of Graphite Oxide and Its Polymer Composite. *J. Am. Chem. Soc.* **2009**, *131* (31), 11027–11032.
- (5) Sun, Y.; He, C. Synthesis and Stereocomplex Crystallization of Poly(lactide)-Graphene Oxide Nanocomposites. *ACS Macro Lett.* **2012**, *1* (6), 709–713.
- (6) Xu, J.-Z.; Liang, Y.-Y.; Zhong, G.-J.; Li, H.-L.; Chen, C.; Li, L.-B.; Li, Z.-M. Graphene Oxide Nanosheet Induced Intrachain Conformational Ordering in a Semicrystalline Polymer. *J. Phys. Chem. Lett.* **2012**, *3* (4), 530–535.
- (7) Li, Y.; Umer, R.; Samad, Y. A.; Zheng, L.; Liao, K. The effect of the ultrasonication pre-treatment of graphene oxide (GO) on the mechanical properties of GO/polyvinyl alcohol composites. *Carbon* **2013**, *55*, 321–327.
- (8) Gao, J.; Bai, H.; Zhou, X.; Yang, G.; Xu, C.; Zhang, Q.; Chen, F.; Fu, Q. Observation of strong nano-effect via tuning distributed architecture of graphene oxide in poly(propylene carbonate). *Nanotechnology* **2014**, *25* (2), 025702.
- (9) Lalwani, G.; Henslee, A. M.; Farshid, B.; Lin, L.; Kasper, F. K.; Qin, Y.-X.; Mikos, A. G.; Sitharaman, B. Two-Dimensional Nanostructure-Reinforced Biodegradable Polymeric Nanocomposites for Bone Tissue Engineering. *Biomacromolecules* **2013**, *14* (3), 900–909.
- (10) Sun, Y.; He, C. Synthesis and stereocomplex crystallization of poly(lactide)-graphene oxide nanocomposites. *ACS Macro Lett.* **2012**, *1*, 709–713.
- (11) Huang, H.-D.; Xu, J.-Z.; Fan, Y.; Xu, L.; Li, Z.-M. Poly(L-lactic acid) crystallization in a confined space containing graphene oxide nanosheets. *J. Phys. Chem. B* **2013**, *117*, 10641–10651.
- (12) Liang, Y.-Y.; Yang, S.; Jiang, X.; Zhong, G.-J.; Xu, J.-Z.; Li, Z.-M. Nucleation ability of thermally reduced graphene oxide for polylactide: role of size and structural integrity. *J. Phys. Chem. B* **2015**, *119*, 4777–4787.
- (13) Xu, H.; Wu, D.; Yang, X.; Xie, L.; Hakkarainen, M. Thermostable and Impermeable “Nano-Barrier Walls” Constructed by Poly(lactic acid) Stereocomplex Crystal Decorated Graphene Oxide Nanosheets. *Macromolecules* **2015**, *48* (7), 2127–2137.
- (14) Xu, H.; Feng, Z.; Xie, L.; Hakkarainen, M. Graphene Oxide-Driven Design of Strong and Flexible Biopolymer Barrier Films: From Smart Crystallization Control to Affordable Engineering. *ACS Sustainable Chem. Eng.* **2015**, DOI: [10.1021/acssuschemeng.Sb01273](https://doi.org/10.1021/acssuschemeng.Sb01273).
- (15) Hua, L.; Kai, W.; Inoue, Y. Synthesis and characterization of poly(epsilon-caprolactone)-graphite oxide composites. *J. Appl. Polym. Sci.* **2007**, *106*, 1880–1884.
- (16) Sayyar, S.; Murray, E.; Thompson, B. C.; Gambhir, S.; Officer, D. L.; Wallace, G. G. Covalently linked biocompatible graphene/polycaprolactone composites for tissue engineering. *Carbon* **2013**, *52*, 296–304.
- (17) Murray, E.; Sayyar, S.; Thompson, B. C.; Gorkin, R., III; Officer, D. L.; Wallace, G. G. A bio-friendly, green route to processable, biocompatible graphene/polymer composites. *RSC Adv.* **2015**, *5*, 45284–45290.
- (18) Murray, E.; Thompson, B. C.; Sayyar, S.; Wallace, G. G. Enzymatic degradation of graphene/caprolactone materials for tissue engineering. *Polym. Degrad. Stab.* **2015**, *111*, 71–77.
- (19) Wan, C.; Chen, B. Poly(epsilon-caprolactone)/graphene oxide biocomposites: mechanical properties and bioactivity. *Biomed. Mater.* **2011**, *6* (5), 055010.
- (20) Hassanzadeh, S.; Aminlashgari, N.; Hakkarainen, M. Chemo-selective high yield microwave assisted reaction turns cellulose to green chemicals. *Carbohydr. Polym.* **2014**, *112* (0), 448–457.
- (21) Hassanzadeh, S.; Aminlashgari, N.; Hakkarainen, M. Microwave-assisted recycling of waste paper to green platform chemicals and carbon nanospheres. *ACS Sustainable Chem. Eng.* **2015**, *3*, 177–185.
- (22) Wu, D.; Hakkarainen, M. A Closed-loop Process from Microwave-assisted Liquefaction of Starch to Utilization of the Liquefaction Products as Starch Plasticizers. *ACS Sustainable Chem. Eng.* **2014**, *2*, 2172–2181.
- (23) Adolfsson, K. H.; Hassanzadeh, S.; Hakkarainen, M. Valorization of cellulose and waste paper to graphene oxide quantum dots. *RSC Adv.* **2015**, *5* (34), 26550–26558.
- (24) Hassanzadeh, S.; Adolfsson, K. H.; Hakkarainen, M. Controlling the cooperative self-assembly of graphene oxide quantum dots in aqueous solutions. *RSC Adv.* **2015**, *5* (71), 57425–57432.
- (25) Koenig, M. F.; Huang, S. J. Biodegradable blends and composites of polycaprolactone and starch derivatives. *Polymer* **1995**, *36* (9), 1877–1882.
- (26) Scherrer, P. Bestimmung der Größe und der inneren Struktur von Kolloideiteilchen mittels Röntgenstrahlen. *Nachr. Ges. Wiss. Goettingen, Math.-Phys. Kl.* **1918**, *1918*, 98–100.
- (27) Kokubo, T.; Ito, S.; Huang, Z. T.; Hayashi, T.; Sakka, S.; Kitsugi, T.; Yamamuro, T. Ca, P-rich layer formed on high-strength bioactive glass-ceramic A-W. *J. Biomed. Mater. Res.* **1990**, *24* (3), 331–343.
- (28) Kokubo, T.; Kushitani, H.; Sakka, S.; Kitsugi, T.; Yamamuro, T. Solutions able to reproduce *in vivo* surface-structure changes in bioactive glass-ceramic A-W3. *J. Biomed. Mater. Res.* **1990**, *24* (6), 721–734.
- (29) Kim, H.; Abdala, A. A.; Macosko, C. W. Graphene/Polymer Nanocomposites. *Macromolecules* **2010**, *43* (16), 6515–6530.
- (30) Balkova, R.; Hermanova, S.; Voberkova, S.; Damborsky, P.; Richtera, L.; Omelkova, J.; Jancar, J. Structure and Morphology of Microbial Degraded Poly( $\epsilon$ -caprolactone)/Graphite Oxide Composite. *J. Polym. Environ.* **2014**, *22* (2), 190–199.
- (31) Gupta, K. K.; Kundan, A.; Mishra, P. K.; Srivastava, P.; Mohanty, S.; Singh, N. K.; Mishra, A.; Maiti, P. Polycaprolactone composites with TiO<sub>2</sub> for potential nanobiomaterials: tunable properties using different phases. *Phys. Chem. Chem. Phys.* **2012**, *14* (37), 12844–53.
- (32) Depan, D.; Pesacreta, T. C.; Misra, R. D. K. The synergistic effect of a hybrid graphene oxide-chitosan system and biomimetic mineralization on osteoblast functions. *Biomater. Sci.* **2014**, *2* (2), 264–274.
- (33) Liu, H.; Cheng, J.; Chen, F.; Hou, F.; Bai, D.; Xi, P.; Zeng, Z. Biomimetic and Cell-Mediated Mineralization of Hydroxyapatite by Carrageenan Functionalized Graphene Oxide. *ACS Appl. Mater. Interfaces* **2014**, *6* (5), 3132–3140.
- (34) Chen, S.; Zhu, J.; Wu, X.; Han, Q.; Wang, X. Graphene Oxide–MnO<sub>2</sub> Nanocomposites for Supercapacitors. *ACS Nano* **2010**, *4* (5), 2822–2830.